Optics and Laser Technology 131 (2020) 106416

Contents lists available at ScienceDirect

Optics and Laser Technology

journal homepage: www.elsevier.com/locate/optlastec

Full length article

Laser printing of silver-based micro-wires in ZrO_2 substrate for smart implant applications

C.G. Moura[a,*], D. Faria[a], O. Carvalho[a], R.S.F. Pereira[e], M.F. Cerqueira[b,c], R.M. Nascimento[d], F.S. Silva[a]

[a] CMEMS, Universidade do Minho, Campus de Azurém, 4800-058 Guimarães, Portugal
[b] Centro de Física, Universidade do Minho, Campus de Gualtar, 4710-057 Braga, Portugal
[c] InternationalIberian Nanotechnology Laboratory (INL), 4715 Braga, Portugal
[d] Materials Engineering Department, UFRN, 59078-970 Natal, Brazil
[e] Federal Institute of Santa Catarina, IFSC, 88020-300 Florianópolis-SC, Brazil

HIGHLIGHTS

- A hybrid approach for printing micro-wires on zirconia substrate were presented.
- The resistivity of the micro-wires was assessed by the four-probe method.
- The mechanical performance of zirconia before and after wire printing was presented.
- Laser technology was successfully used both to create channel and sinter silver powder inside them.

ARTICLE INFO

Keywords:
Nd:YAG laser
Zirconia implants
Smart implants
Communication systems
Laser sintering

ABSTRACT

Smart implants are endowed with functions of sensing, actuating and control to solve problems that may arise during their use. The assembly of these functions along the implant surface is still a challenge. However, with the advent of 3D printing, it is possible to print on implants' surface, communication channels or micro-antennas or even sensoric/actuating areas. Hence, a positive impact on the long-term performance of the implants (including hip, dental and knee) may be expected with the proposed approach. Despite titanium and Ti6Al4V titanium alloy are the standard choice for implants fabrication, 3Y-TZP (tetragonal 3% mol yttria-stabilized zirconia) has emerged as a ceramic material suitable to overcome titanium alloy problems, due to its numerous advantages. In this sense, this work is concerned with the ability of printing silver-based communication system in zirconia substrates by using laser technology. For this purpose, micro-cavities were created on ZrO_2 substrate, where the silver powder was placed and sintered into them. Through the laser approach, silver-based wires with great quality and low resistivity values were achieved. The flexural strength results showed that the mechanical resistance of zirconia disks was affected by laser micro-wire printing, which decreased as the laser passage was performed. Based on the results, it is believed that the proposed approach seems to be effective for the manufacturing of implants with intrinsic capacities, useful for smart implant applications.

1. Introduction

Smart active implants incorporate functions of sensing, actuation, and control in order to describe and analyze a situation and make decisions based on the available data in a predictive or adaptive manner, thereby performing smart actions [1,2]. These implants need to have sensors, actuators, and communication cavities such as electrical wires and antennas as illustrated in Fig. 1.

However, the assembling of these elements along the implant surface is difficult and will modify some desired characteristics of the implant for implantation, osseointegration, etc. Nevertheless, with the advent of 3D printing, mainly with multi-material approaches, it is possible to print, layer by layer, implants where a communication system, mimicking the central nervous system of lining bodies, local materials as sensors or actuators, such as piezo electric materials (for instance $BaTiO_3$), among other, may be successively printed giving rise

* Corresponding author at: CMEMS-Uminho, Universidade do Minho, Campus de Azurém, 4800-058 Guimarães, Portugal.
E-mail address: caroline.materiais@gmail.com (C.G. Moura).

https://doi.org/10.1016/j.optlastec.2020.106416
Received 9 September 2019; Received in revised form 28 May 2020; Accepted 8 June 2020
Available online 26 June 2020
0030-3992/

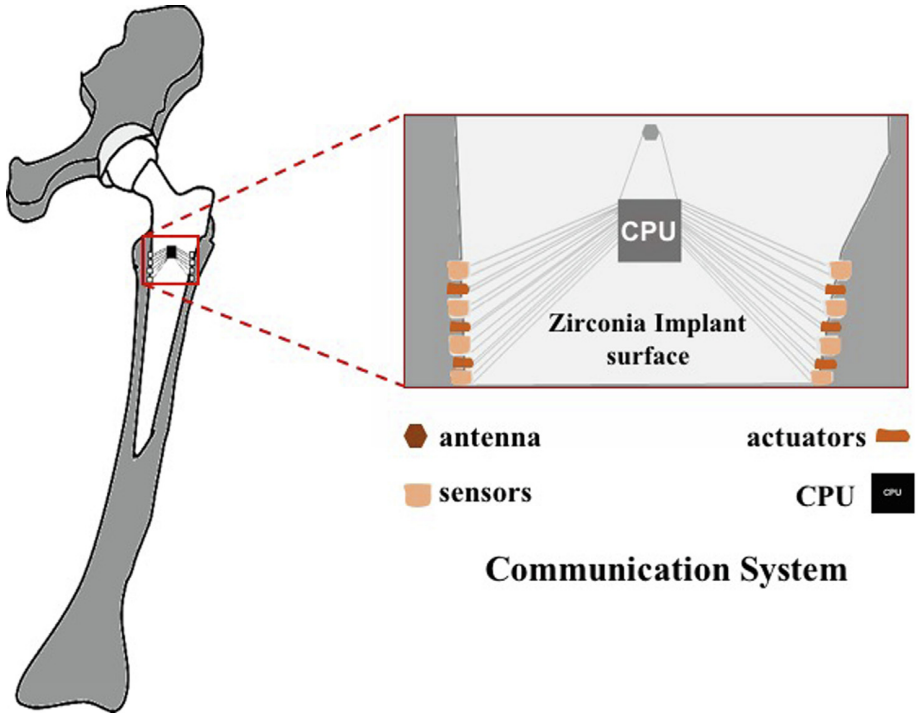

Fig. 1. Schematic illustration of a zirconia implant with smart devices printed along the implant surface. Modified from [3].

to a component with an internal communication array of wires and local surface areas with ability to sense (temperature, PH, etc.) and or actuate (with electrical potentials, volume changing). It is also possible to print, on the implant's surface, communication cavities, or micro-antennas, or even sensoric/actuating areas.

This new concept of one component active implant with intrinsic smart functions, similar to biological bodies, is being investigated and manufactured with new complex multi-material 3D printing, which is shown in Fig. 2.

Although titanium and its alloys are the standard choice for biomedical implants fabrication, tetragonal 3 mol% yttria stabilized zirconia (3Y-TZP) has arisen as a promising and eligible ceramic material for implants fabrication to overcome metal ions release and allergic reactions provided from titanium implants which compromise their durability. The main advantages of using zirconia is due to its high chemical and dimensional stability, mechanical strength, relatively good toughness, and low bacterial affinity [4,5].

Until this moment, the studies are focused on dental implants, in which several investigations have demonstrated a good performance of zirconia implants when compared to titanium alloy [6–8]. Several in vivo and in vitro investigations of soft tissue responses around zirconia revealed comparable or even better healing response, less inflammatory infiltrate and reduced plaque adhesion on zirconia compared to conventionally pure titanium [9–11]. Despite this, the drive towards ceramic implants to satisfy the increasing aesthetic demands and metal-free request is fraught with compromise. According to literature, there is still no valid scientific data available to recommend the routine clinical use of zirconia implants since the majority of the studies are either case reports or case series with a limited number of participants and short-term follow-up periods [8]. Furthermore, since zirconia is a brittle material with significant sensitivity to the surface defects, good control of quality during the manufacturing process is a necessity to enhance the long-term performance of the zirconia implants [12,13]. Based on the foregoing, this work is concerned with the ability of printing silver-based communication system in zirconia substrates by using laser technology.

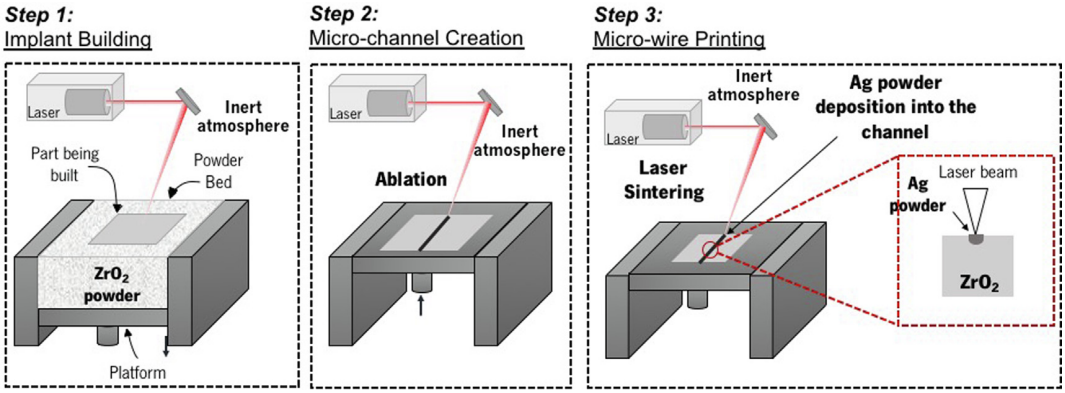

Fig. 2. Illustrative scheme of the manufacturing steps of the micro-wires by 3D printing.

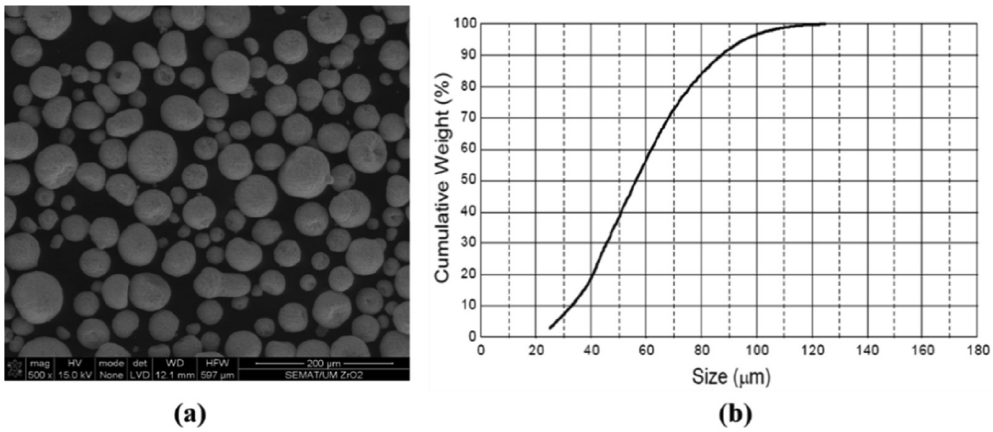

Fig. 3. TZ-3YSB-E powder: (a) SEM image and (b) cumulative weight distribution curve as a function of size (according to manufacturer).

2. Materials and methodology

2.1. Zirconia disks fabrication

A commercial powder of 3% mol yttria stabilized zirconia – 3Y-TZP (TZ-3YSB-E Tosoh Corporation, Japan) having a mean agglomerates size of 60 μm and containing small crystallites of about 36 nm in diameter was used as feedstock to produce zirconia disks by press and sintering technique. Fig. 3a and b present the Scanning Electron Microscopy image of TZ-3YSB-E powder in agglomerate form and the cumulative weight distribution curve as a function of powder size (according to manufacturer), respectively.

The pressing of the TZ-3YSB-E powder was performed on a steel cylindrical mold with an internal diameter of 18 mm and 30 mm of height. First, 2.0 g of TZ-3YSB-E powder was placed into the mold and a pressure of 200 MPa was applied for 30 s [13,14]. After that, the zirconia disks were sintered using a high-temperature furnace (Zirkonofen 700, Zirkonzahn, Italy) with a sintering temperature of 1500°C, a heating and cooling rate of 8 °C/min and 2 h of holding time. After sintering, zirconia disks with 14.4 mm in diameter and 1.8 mm thick were obtained. All disks were ultrasonically cleaned in isopropyl alcohol for 10 min. to remove any loose debris or surface contamination.

2.2. Micro-cavities production

2.2.1 Surface laser texturing

A pulsed Nd:YAG laser (OEM Plus, working in wavelength of 1064 nm) with an output power of 6 W and a spot size of 3 μm was used to produce the micro cavity in the surface of a 1.8 mm thick ZrO_2 disk. Fig. 4 shows a schematic illustration of the experimental set-up of the laser processing. Firstly, the cavity was defined by using a computer-aided design system and then, it was engraved on the zirconia surfaces. The width of the cavity was projected to have 200 μm, as indicated in the Fig. 4a. To create the micro cavity, the laser beam progresses through spiral lines (which are represented by Fig. 4b. These spiral lines are separated with a distance (designated by spacing line) which in turn, vary from 10 to 50 μm, as presented in Fig. 4b. The laser specifications are tabulated in Table 1.

Fig. 5 presents a diagram that illustrates the definition of the overlapping of laser spots at the focusing plane of the converging lens.

The number of pulses is 12 and the overlapping percentage of two consecutives pulses is 91,6%. Both values were obtained through Eq. (1) [14] and (2) [15], as following. The laser parameters used in the Eqs. (1) and (2) are presented in Table 1.

$$N = \frac{2\omega}{d} \tag{1}$$

where N is the number of pulses, ω is the laser spot radius, d is the distance between consecutive laser pulse.

$$O\% = \frac{D-d}{D} \times 100 \quad d = \frac{v}{f} \tag{2}$$

where v is the scanning speed and f is the laser pulse repetition frequency.

Three laser scanning parameters were varied in this study, namely laser power, scanning speed and number of passes, in order to evaluate (i) their influence on the quality of the cavity, (ii) the amount of material re-solidified and (iii) the depth achieved. Laser power represents the laser beam energy delivered per pulse in Watts; the scanning speed is the marking speed at the leading edge of the beam front in mm/s and the number of passes corresponds to the number of scans carried out by the laser during the process, which will affect the depth of the groove. Thus, in this study, the energy density was kept constant while the other parameters varied. Table 2 shows the combination of parameters used in this work.

The laser energy density (E) was calculated for each condition through the equation below:

$$E = \frac{P \times n}{v} \tag{3}$$

where P is the laser power, E is energy density in J/mm^2; n is the number of passes and v is the scanning speed in mm/s.

For each condition, there is a parameter combination in which the energy density corresponds to the same value, 20 J/mm^2. The definition of this energy density value was based on the results available in literature [12,13].

2.3. Micro-wire printing

In the silver (Ag) wire printing, silver powder (≥99% pure) with an average grain size of 230 nm, from Metalor Technologies-USA, was deposited and compacted into the micro-cavity on ZrO_2 substrate. After the deposition, the powder was compacted by using a pressure of 8 MPa to ensure the total accommodation of the powder into the micro-cavity. The excess of the powder on the surface was removed through polishing with P800 grit SiC paper. In order to consolidate the powder into the micro-cavity, a pulsed Nd:YAG (Sisma − 1064 nm of wavelength) with a spot size of 0.3 μm and 100 J of maximum energy has been used. An energy of 10 J was used in all the samples and the process was accomplished with argon, an inert gas, in order to prevent silver oxidation. This value of energy was chosen as the best condition to melt the powder with fewer defects after several parameters' tests. To subject the silver powder to laser beam, the samples were put into the work chamber and the laser beam was focused on the micro-cavity (filled by

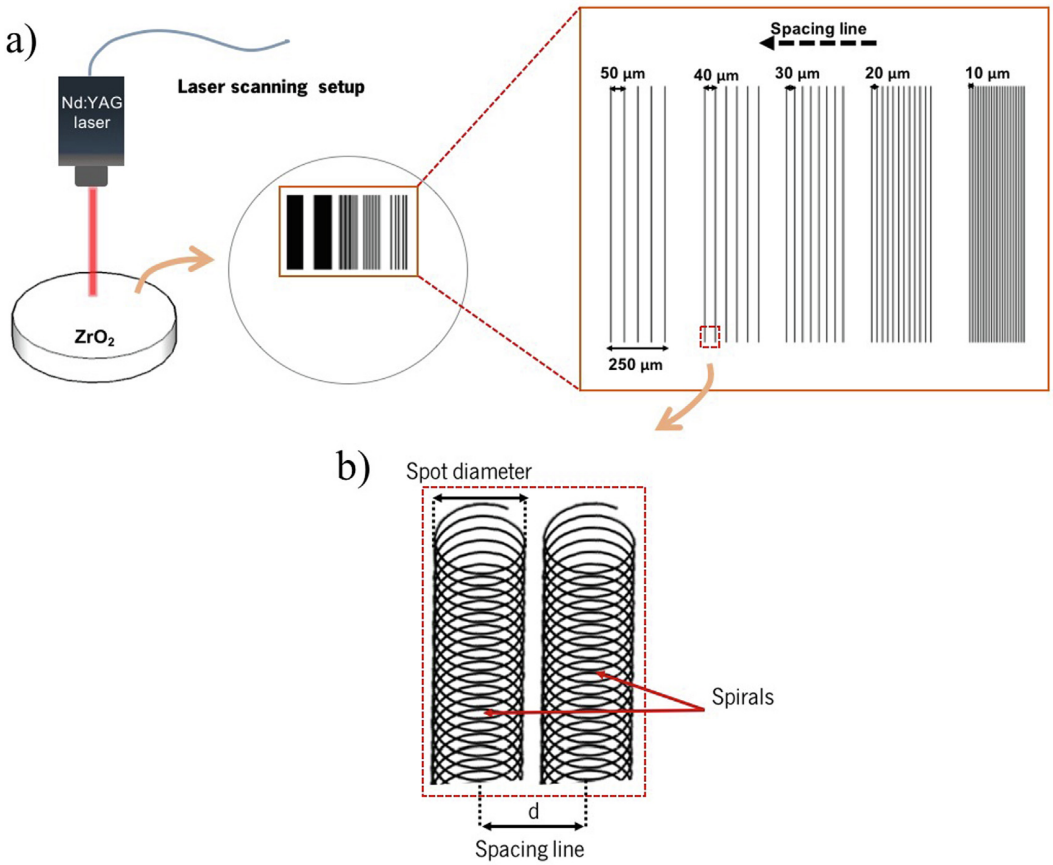

Fig. 4. Scheme illustrating the experimental set-up of the laser processing (a and b).

Table 1
Nomenclature and values of laser parameters.

Laser parameters	
Number of pulses - *N*	12
Radius of laser beam spot size -*ω*	1.5 µm
Distance between consecutive laser pulses - *d*	0.25 µm
Overlapping percentage - *O*	91.6%
Spot diameter - *D*	3 µm
Scanning velocity -*v*	5 mm/s
Laser pulse repetition frequency -*f*	20 KHz

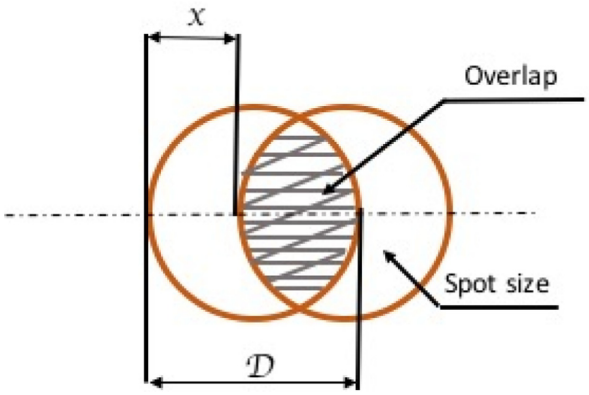

Fig. 5. Depiction of overlapping of laser beams and definition of beam overlapping in the laser micromachining process.

Table 2
Laser parameters combination.

Pack 1			
Sample	Power (W)	Scanning speed (mm/s)	Number of passes
ZrP1.1	6	5	1
ZrP1.2	3	5	2
ZrP1.3	1.5	5	4
ZrP1.4	0.75	5	8
ZrP1.5	0.375	5	16
ZrP1.6	6	25	5
ZrP1.7	3	25	10
ZrP1.8	1.5	25	20
ZrP1.9	0.75	25	40
ZrP1.10	0.375	25	80
Pack 2			
ZrP2.1	6	50	10
ZrP2.2	3	50	20
ZrP2.3	1.5	50	40
ZrP2.4	0.75	50	80
ZrP2.5	0.375	50	160
ZrP2.6	6	100	10
ZrP2.7	3	100	20
ZrP2.8	1.5	100	40
ZrP2.9	0.75	100	80
ZrP2.10	0.375	100	160

silver powder) to be welded. For sintering process, a dual axis automatic worktable was used to position the zirconia disk and for scanning all the cavity in an automatic way, as illustrated in Fig. 6.

The silver wires were characterized by Scanning Electron Microscope (SEM - FEI Nova 200) to evaluate the quality of the wire, in

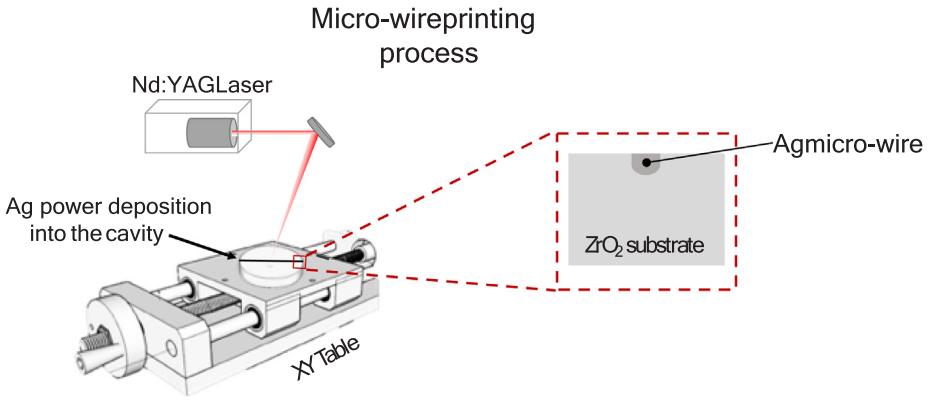

Fig. 6. Schematic representation of the micro-wire printing process.

terms of densification. Energy Dispersive Spectrometer (EDS) was performed to verify the presence of silver oxidation.

2.4. Electrical resistivity of the wires

In order to evaluate the electrical conductivity of the printed silver wires, the four-point probe method has been used. A schematic illustration of this method is presented in Fig. 7. In this method a current is passed through the outer probes and induces a voltage in the inner voltage probes, resulting in a I × V curve. The range of applied current was 0.01 to 0.1 Ampère.

The electrical performance was evaluated by comparing the resistivity (ρ) obtained by the application of Eq. (4), [16]:

$$\rho = R\frac{A}{L} \tag{4}$$

where ρ is the resistivity, R is the resistance measured on the wire, L is the distance between each probe, and A is the cross-sectional area of the Ag wire. To obtain accurate resistivity, the actual cross-sectional area was assumed to be a uniform wire with approximately 200 μm of diameter. This equation for the resistivity calculation is the most adequate because as the wire is deposited in an insulating substrate, the conductivity is supplied by the metal present, since all the current flows through the wire.

2.5. Ball-on-three-balls (B3B) tests

In order to evaluate the effects of the silver wire printing on the zirconia surface regarding mechanical performance, the flexural strength of the samples was measured using the ball-on-three-balls test. The tests were done before the laser irradiation (as sintered sample), after the micro-cavity production by laser and after the silver wire printing on the cavity. The samples were then divided into three groups:

1. Zirconia samples as sintered (ZrAS);
2. Zirconia samples with a micro-cavity produced by laser (ZrP2.7);
3. Zirconia samples with a micro-cavity produced by laser containing a silver wire within the micro-cavity (ZrP2.7_Ag).

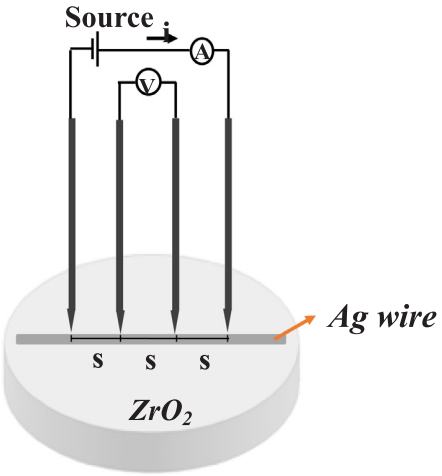

Fig. 7. Schematic representation of the four-probe method.

Tests were performed at room temperature (~23 °C) in a servohydraulic machine (Instron 8874 MA, USA), equipped with a 25 kN capacity load cell at a loading rate of 1 mm/min. In the test, the intended side of the sample was positioned in the sample's holder on top of the three supporting steel balls equidistant from its center. The opposite surface was centrally loaded by a fourth ball coupled to the pin crosshead of the testing machine. The test started from a small preload and then the load increased until sample fracture. After that, the fracture load was recorded and the maximum tensile stress(σ_{max}), that occurs in the centre of the sample, on the opposite side of the loading ball, was calculated according to the Equation (5) [17,18]:

$$\sigma_{max} = \frac{F}{t^2}\left[c_0 + \frac{c_1 + c_2(t/R) + c_3(t/R)^2 + c_4(t/R)^3}{1 + c_5(t/R)}\left(1 + c_6\frac{R}{R_a}\right)\right] \tag{5}$$

where F is the maximum force at fracture (N), t the sample thickness (mm), R the sample radius (mm), R_a the support radius (R_a = 5 mm), and the parameters c0 to c6 refers to fitting factors for the geometrical correction term (c_0 = -17,346 c_1 = 20,774 c_2 = 622.62 c_3 = 76.879 c_4 = 50.383 c_5 = 33.736 c_6 = 0.0613). According to Borger et al. [18], the parameters for c0 to c6 depend on the Poisson's ratio, which for zirconia (t-ZrO_2 with 3 mol.% Y_2O_3) corresponds to $\upsilon = 0.31 \pm 0.01$ [19]. After B3B tests, the fracture surfaces were analyzed by Scanning Electron Microscopy (SEM – FEI Nova 200). For this analysis, the samples were coated with an Au/Pd layer of 3 nm of thickness.

3. Results and discussion

3.1. Surface morphology of the laser micro-cavity

Fig. 8(a and b) shows the scanning electron micrographs of the laser textured surface of ZrO_2 processed in air. Fig. 8a and b represent the textured surfaces produced from Pack 1 and Pack 2 conditions, respectively. Each micrograph is compound by a group of 5 micro-cavities, with a width around 200 μm, wherein each one was built by periodic lines spaced with different values: from 10 to 50 μm - as can be seen in Fig. 4a. For each combination of parameters, the value of energy

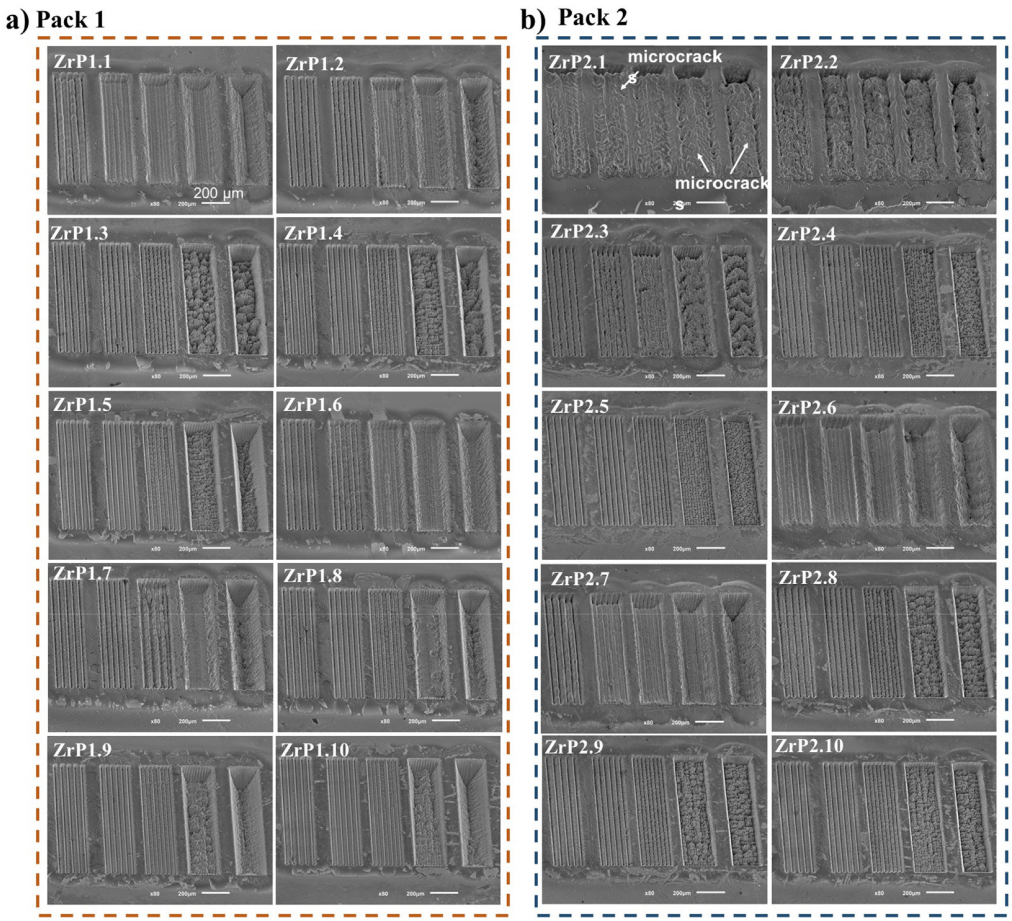

Fig. 8. SEM micrographs of top surface of laser textured ZrO_2 with different parameters combination: (a) pack 1, (b) pack 2. Each textured area has 5 set of micro-cavities formed by lines spaced with different values: from 10 to 50 µm (from left to right). The magnification is 80x and the bar corresponds to 200 µm for all the micrographs.

density is the same and it was chosen based on the reported undesirable effects (such as micro-cracks propagation, spatter and heat-affected zone) after laser irradiation of zirconia surface, in an attempt of minimizing such effects.

However, by analyzing the SEM images in Fig. 8 it is possible to see that each parameter combination results in different surface changes, which means that each parameter has an important role in the surface modification.

In general, the laser scanning produced tracks of approximately 250 µm of width formed by overlapped lines and, for the same energy density, different surface morphologies can be obtained by combining different laser parameters. According to the images in Fig. 8, the line spacing above 40 µm did not result in a micro-cavity formation, but a set of spaced tracks. However, for printing the wire, it is necessary to create a clean micro-cavity with considerable depth and therefore, only conditions 20 and 10 µm of spacing lines met these requirements. By analyzing the other parameters, in pack 1, from condition ZrP1.6, by increasing the scanning speed, the groove becomes cleaner and presents higher depth. However, in the conditions in which the scanning speed is lower (ZrP1.1 to ZrP1.5), the decrease of laser power is compensated by the increase of laser passes, resulting in micro-cavities with a great amount of re-solidified material droplets (debris) accumulated into the tracks. On the other hand, in pack 2, in which the scanning speed is higher, and more laser passes were performed, damaged surfaces were obtained in the conditions ZrP2.1 and ZrP2.2, presenting microcracks and holes on the surface, since higher output power is used. In general, only two conditions tested in this pack resulted in a desirable micro-cavity (ZrP2.6 and ZrP2.7), from the combination of high scanning speed and laser power with less laser passes. This result was already mentioned in previous studies, which reported the observation of microcracks on the zirconia surface after Nd:YAG treatment [20–22]. The presence of microcracks is a consequence of thermal gradients provided by rapid cooling during the laser irradiation. In literature, different methods to machining ceramics by laser for defect-free have been tested, for instance, underwater processing [23,24].

When the laser beam reaches a ceramic surface, physical phenomena take place, namely reflection, absorption, scattering and transmission. Absorption is the vital of all the effects, it is the interaction of the electromagnetic radiation with the electrons of the material and it depends on both the wavelength of the material and the spectral absorptivity characteristics of the ceramic being machined [25]. Furthermore, as the thermal conductivity of ceramics is generally less comparing to the majority of metals, the energy absorption takes place faster in ceramics and all the incident energy is immediately absorbed by the ceramic for the machining process [25–27].

Thereby, when the material is subjected to large enough incident laser energy, the temperature of the surface can surpass the boiling point of the material promoting rapid vaporization and subsequent material removal by the process referred to as ablation. This process takes place when the minimum energy required to remove material is achieved, and it depends on the interaction between the photo-thermal and photo-chemical (bond breaking) mechanisms [25].

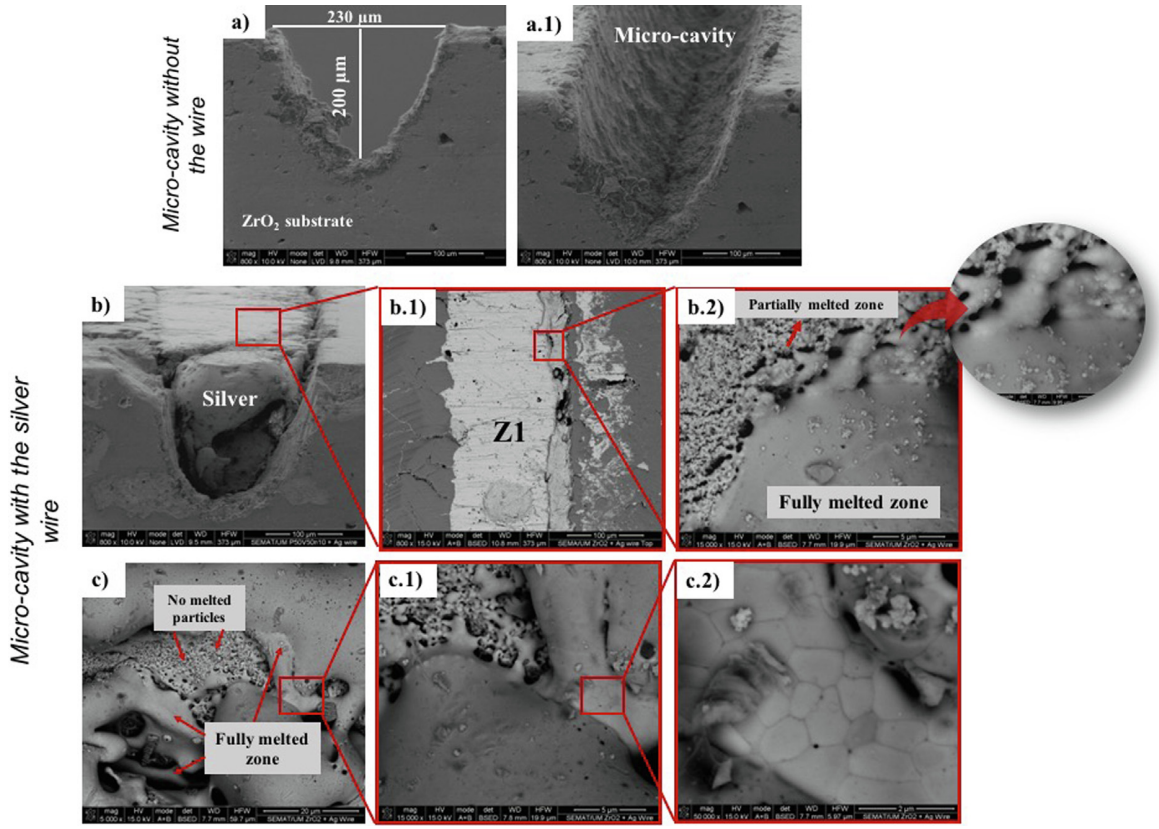

Fig. 9. SEM micrographs of: (a) Micro-cavity before the silver wire printing, obtained after laser machining. (b) and (c) Micro-wire printed into the cavity through laser sintering process, with marked zone (Z1) for EDS analysis.

3.2. Silver wire printing

After studying laser parameters for the micro-cavities production on zirconia surface, the condition ZrP2.7 was chosen for printing the micro-wire, since this condition resulted in a cleaner micro-cavity with a desirable depth. Fig. 9a presents SEM micrographs of the micro-cavity obtained after laser machining, before the silver wire printing. Fig. 9b and c show the micro-wire printed into the cavity through laser sintering process.

As can be observed, the silver powder grains were apparently melted and spread to completely merge together with neighboring grains. However, regions where the powder was not fully consolidated is also observed, as well as zones with necks formation between the particles. In laser sintering, localized energy is deposited, in which the powder is selectively irradiated and locally sintered, while the non-irradiated part of the laser stays unconsolidated [28], as occurred in our case. Another important aspect regarding laser sintering is related to a very steep temperature gradient that is generated due to the fast heating and cooling rate during the process. Because of the temperature gradient, during laser sintering of the wire, thermal stresses are generated due to the expansion restriction of the heated top layer, promoting compressive stresses. On the other hand, there is a contraction of the top layer of the metal powder, while the laser scans the surface, which is also restricted by the surrounding area, leading to tensile residual stress, being accumulated and resulting in cracks formation and delamination [29,30]. The EDS analysis of the silver wire (Z1), presented in Fig. 10, confirms the presence of the Ag element and the absence of oxygen.

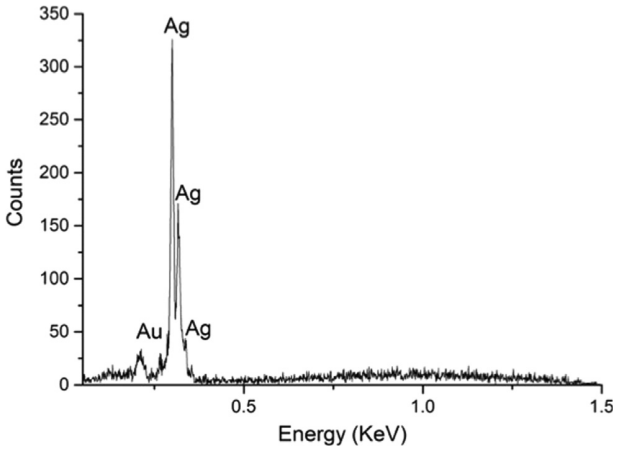

Fig. 10. EDS analysis of the silver wire marked as Z1 on Fig. 9b.1.

3.3. Electrical resistance measurements of the wires

After silver wire printing in the zirconia surface, electrical measurements were performed in order to evaluate their ability to conduct electrical current. For this purpose, the four-point probe method has been used by applying an electrical current and measuring the voltage resultant. Fig. 11 presents the VxI curves of three samples prepared with the same conditions and their respective resistance values.

Thus, assuming a uniform wire with known dimensions, the resistivity (ρ) of the silver wire can be calculated through VxI curves by using Eq. (2) and the values are presented in Fig. 11. The values of electrical resistivity for zirconia and silver at room temperature,

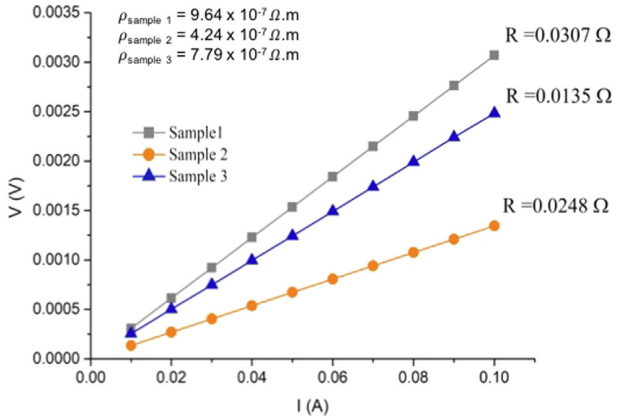

Fig. 11. VxI curves with the resistance and the electrical resistivity values of each sample measured.

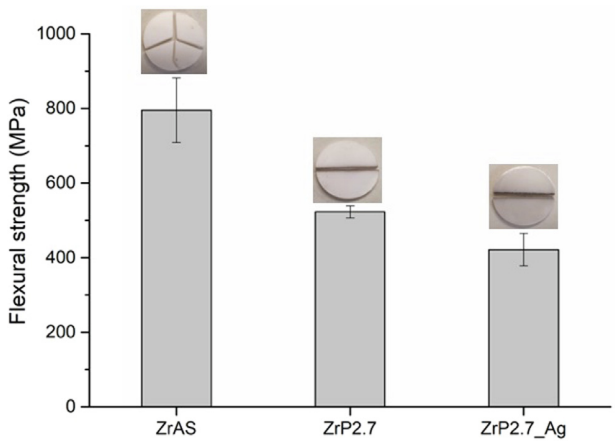

Fig. 12. Mean flexural strength obtained from the ball-on-three-balls (B3B) test and the corresponding fragments of broken ZrAS, ZrP2.7 and ZrP2.7_Ag samples.

according to literature are 10^{12} [31] and 1.6 × 10^{-8} ohm.m [32], respectively. According to the results, the electrical resistivity values for the produced wires presented one order of magnitude higher than the theoretical value of silver. This outcome was expected since imperfections (such as impurities and discontinuities), resulting from the sintering process, may hamper the mean free path of electrons, contributing for the resistivity increase. Such imperfection can be also related to the presence of porous. As it is well-known the sintering process is the atom diffusion driven by internal and external energies or forces. A denser microstructure would enhance the electrical conductivity, which indicates that good densification in the sintering process is a key to secure better electrical properties [33].

To date, the process of printing electronic devices and circuits in insulator substrates is already quite developed. However, the main processes of manufacturing involve high temperature and pressure in traditional sintering approaches, which are not tolerated by the soft substrates commonly used. Although several room-temperature and pressureless methods have been proposed, these methods are based on the use of chemical agents, compromising the electrical performance [33–36]. Thus, works related with printing local conductive cavities by using a single method (laser technology) are very scarce. Our proposed method allows, through a single technology, to print conductive wires on the surface of a zirconia implant, endowing it with diverse capabilities. The micro-wires printed by this methodology presented desirable electrical performance for the intended application.

3.4. Flexural strength results

In order to evaluate the influence of the micro-wires printing on the mechanical strength of zirconia, ball on three balls tests were performed. The laser irradiation is known to affect the ceramics mechanical properties and, therefore, zirconia substrate was tested before and after each laser modification [37]. Despite its importance, in literature, studies related to this aspect are very scarce. In Noda et al. [38], they presented the characterization of the surface damages of zirconia irradiated by Nd:YAG laser and the microstructural changes. The results revealed that cracks were formed after laser treatment and oxygen loss occurred. However, any mechanical property has been investigated in their study. Carvalho et al. [39] also presented an investigation regarding the influence of laser parameters and irradiation atmosphere on ZrO_2 surface. The main objective was to create cavities and functionalize them with bioactive materials for zirconia surface bioactivity improvement. Despite their satisfactory results of bioactive adhesion, the mechanical properties of zirconia after laser irradiation was not assessed.

According to the ISO 13356:2008 (Implants for surgery – ceramic materials based on yttria-stabilizes tetragonal zirconia (Y-TZP)), the flexural strength of zirconia should be ≥500 MPa [40]. In Fig. 12 are shown the mean flexural strength values obtained from the B3B tests for each group of samples as well as the corresponding fractured samples.

Analyzing the obtained results, a flexural strength value of 795 ± 87 MPa was obtained for ZrAS samples, which is in agreement with the standard defined by the ISO 13356:2008. Within the laser irradiated samples, there was a decrease in flexural strength values from 523 ± 16 MPa to 422 ± 43 MPa for ZrP2.7 and ZrP2.7_Ag samples, respectively. Additionally, by comparing flexural strength values of ZrP2.7 and ZrP2.7_Ag samples with ZrAS samples, a decrease was verified. This means that the mechanical resistance of zirconia was affected by the laser surface irradiation. Despite this reduction on the flexural strength values, it is important to highlight, that the value of ZrP2.7 samples is within the standard defined by the ISO 13356:2008. Regarding the ZrP2.7_Ag value, this found below of the one defined by the ISO 13356:2008. Reasons may lie on the fact of surfaces have been subjected twice times to the laser irradiation (laser ablation and laser sintering processes), while in the case of ZrP2.7 samples the surfaces were irradiated by laser one time in the step of micro-cavity production (laser ablation process), therefore, the mechanical performance was less compromised. Additionally, it is worth noting that the flexural strength value stated by the ISO 13356:2008 is defined for a zirconia sample without any surface treatment and in our study, the surface of the samples was irradiated by laser. Thus, it is expectable a decrease in flexural strength values after laser irradiation. Although Nd:YAG pulsed laser has demonstrated to be adequate to scan the ceramic surface, due to the fast heat and cooling generated in laser scanning, the ceramic surface is damaged.

Fig. 13 presents the fracture surface of each group of samples. It can be seen from Fig. 13a and b that, in all group of samples, the failure started from the bottom part of the samples, which corresponds to the tensile surface in the B3B test. The fracture surfaces exhibited typical fracture patterns of ceramic materials [41]. Additionally, it can be observed from Fig. 13 that the fracture surfaces revealed the absence of detectable porosity within the samples.

4. Conclusions

This study proposes a novel approach for fabrication of zirconia-based implants with intrinsic capacities, through the laser printing of a communication system. Laser was employed as a versatile tool for modifying the material surface, whether to create the micro-cavities, in a subtractive way, and for consolidate the micro-wires, in an additively way. The micro-wires printed by the proposed method exhibited low values of electrical resistance and a resistivity of 10^{-7} Ω.m, being a

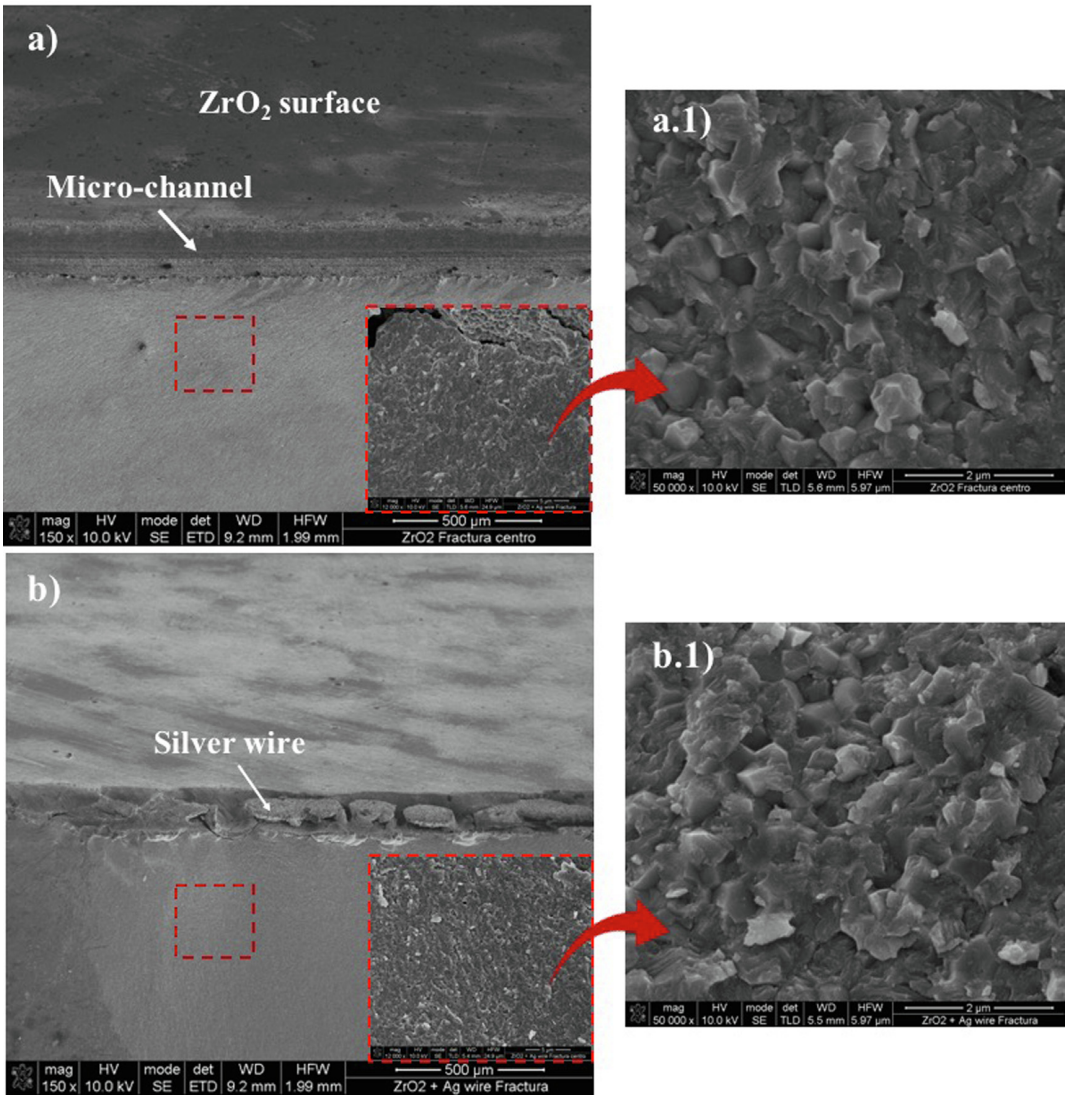

Fig. 13. SEM micrographs of fracture surfaces of the samples: (a) and (a.1) ZrP2.7 and (b) and (b.1) ZrP2.7_Ag, after ball-on-three-balls (B3B) test.

conductor path to the electrical flow.

The flexural strength of zirconia presented a decrease as the laser passage was performed, from 795 to 523 and 422 MPa, for the "as sintered" sample (ZrAS), for the sample with the micro-cavity (ZrP2.7) and for the sample after the micro-wire printing (ZrP2.7_Ag), respectively. According to ISO 13356:2008, the samples after the micro-wire printing presented a value of flexural strength just below the standard requirement of 500 MPa. However, further mechanical tests could be performed to allow a deeper understanding of the laser action on the zirconia surface.

CRediT authorship contribution statement

C.G. Moura: Conceptualization, Methodology, Validation, Investigation, Writing - original draft, Writing - review & editing. **D. Faria:** Methodology, Validation, Writing - review & editing. **O. Carvalho:** Supervision, Software. **R.S.F. Pereira:** Methodology, Writing - review & editing. **M.F. Cerqueira:** Resources, Writing - review & editing. **R.M. Nascimento:** Supervision. **F.S. Silva:** Supervision, Project administration, Resources.

Declaration of Competing Interest

The authors declare that they have no known competing financial interests or personal relationships that could have appeared to influence the work reported in this paper.

Acknowledgement

This work has been supported by FCT (Fundação para a Ciência e Tecnologia - Portugal) in the scope of the projects UID/EEA/04436/2019 and NORTE-01-0145-FEDER-000018-HAMaBICo and Add.Additive_Manufacturing to Portuguese Industry_POCI-01-0247-FEDER-024533. Thank the CNPq (205791/2014-0) and CAPES for the financial support.

References

[1] E.H. Ledet, B. Liddle, K. Kradinova, S. Harper, Smart implants in orthopedic surgery , improving patient outcomes : a review, (2018) 41–51.
[2] C. O'Connor, A. Kiourti, Wireless Sensors for Smart Orthopedic Implants, J. Bio-Tribo-Corrosion. 3 (2017) 1–8, https://doi.org/10.1007/s40735-017-0078-z.
[3] C.G. Moura, O. Carvalho, L.M.V. Gonçalves, M.F. Cerqueira, R. Nascimento, F. Silva, Laser surface texturing of Ti-6Al-4V by nanosecond laser : Surface

characterization, Ti-oxide layer analysis and its electrical insulation performance, Mater. Sci. Eng. C 104 (2019) 109901, , https://doi.org/10.1016/j.msec.2019.109901.
[4] N. Cionca, D. Hashim, A. Mombelli, Zirconia dental implants: where are we now, and where are we heading? Periodontol. 2000 (73) (2017) 241–258, https://doi.org/10.1111/prd.12180.
[5] C.M.L. Bollen, Zirconia : The Material of Choice in Implant Dentistry? An Update, J. Dent. Heal. Oral Disord. Ther. 6 (2017) 1–4, https://doi.org/10.15406/jdhodt.2017.06.00219.
[6] D. Faria, J.M. Pires, A.R. Boccaccini, O. Carvalho, F.S. Silva, J. Mesquita-Guimarães, Development of novel zirconia implant's materials gradated design with improved bioactive surface, J. Mech. Behav. Biomed. Mater. 94 (2019) 110–125, https://doi.org/10.1016/j.jmbbm.2019.02.022.
[7] R. Depprich, H. Zipprich, M. Ommerborn, C. Naujoks, H.-P. Wiesmann, S. Kiattavorncharoen, H.-C. Lauer, U. Meyer, N.R. Kübler, J. Handschel, Osseointegration of zirconia implants compared with titanium: an in vivo study, Head Face Med 4 (1) (2008) 30.
[8] R.B. Osman, M. V Swain, P. Dentistry, S.D. Hospital, S. Hills, A Critical Review of Dental Implant Materials with an Emphasis on Titanium, (2015) 932–958. doi:10.3390/ma8030932.
[9] Y.H. Pae, A. Lee, H. Kim, H.S.Y.D. Woo, Attachment and growth behavior of human gingival fibroblasts on titanium and zirconia ceramic surfaces, Biomed. Mater. 2 (2009) 025005–025012, https://doi.org/10.1088/1748-6041/4/2/025005.
[10] A. Degidi, M. Artese, L. Scarano, A. Perrotti, V. Gehrke, P. Piattelli, Inflammatory infiltrate, microvessel density, nitric oxide synthase expression, vascular endothelial growth factor expression, and proliferative activity in peri-implant soft tissues around titanium and zirconium oxide healing caps, J. Periodontol. 77 (2006) 73–80, https://doi.org/10.1902/jop.2006.77.1.73.
[11] M. Größner-Schreiber, B. Herzog, M. Hedderich, J. Dück, A. Hannig, M. Griepentrog, Focal adhesion contact formation by fibroblasts cultured on surface-modified dental implants: An in vitro study, Clin. Oral Implant. Res. 17 (2006) 736–745, https://doi.org/10.1111/j.1600-0501.2006.01277.x.
[12] L. Liu, S. Liu, X. Song, Effect of Nd : YAG laser irradiation on surface properties and bond strength of zirconia ceramics, (2015) 627–634. doi:10.1007/s10103-013-1381-7.
[13] R.S.F. Pereira, C.G. Moura, B. Henriques, J. Chevalier, F.S. Silva, M.C. Fredel, Influence of laser texturing on surface features, mechanical properties and low-temperature degradation behavior of 3Y-TZP, Ceram. Int. (2019), https://doi.org/10.1016/j.ceramint.2019.10.065.
[14] N.B. Dahotre, S.R. Paital, A.N. Samant, C. Daniel, Wetting behaviour of laser synthetic surface microtextures on Ti-6Al-4V for bioapplication, Philos. Trans. R. Soc. A Math. Phys. Eng. Sci. 368 (2010) 1863–1889, https://doi.org/10.1098/rsta.2010.0003.
[15] J. Marczak, Micromachining and pattering in micro/nano scale on macroscopic areas, Arch. Metall. Mater. 60 (2015) 2221–2234, https://doi.org/10.1515/amm-2015-0368.
[16] E.M. Girotto, I.A. Santos, Medidas de Resistividade Elétrica DC em Sólidos: Como Efetuá-las Corretamente, Quim. Nova. 25 (2002) 639–647, https://doi.org/10.1590/S0100-40422002000400019.
[17] S.L. Stares, M.C. Fredel, P. Greil, N. Travitzky, Paper-derived hydroxyapatite, Ceram. Int. 39 (2013) 7179–7183, https://doi.org/10.1016/j.ceramint.2013.02.062.
[18] A. Borger, P. Supancic, R. Danzer, The ball on three balls test for strength testing of brittle discs: Part II: analysis of possible errors in the strength determination, J. Eur. Ceram. Soc. 24 (2004) 2917–2928, https://doi.org/10.1016/j.jeurceramsoc.2003.10.035.
[19] W. Pabst, G. Tichá, E. Gregorová, Effective elastic properties of alumina-zirconia composite ceramics - Part 3 Calculation of elastic moduli of polycrystalline alumina and zirconia from monocrystal data, Ceramics-Silikáty 48 (2004) 41–48.
[20] M.P. Paranhos, L.H. Burnett Jr, Effect of Nd: YAG laser and CO2 laser treatment on the resin bond strength to zirconia ceramic, Quintessence Int. 42 (2011) 79–89.
[21] B.F. Akyıl, M.S. Uzun, I.H. Bond, strength of resin cement to yttrium-stabilized tetragonal zirconia ceramic treated with air abrasion, silica coating, and laser irradiation, Photomed Laser Surg. 28 (2010) 801–808.
[22] C.G. Moura, R. Pereira, M. Buciumeanu, O. Carvalho, F. Bartolomeu, R. Nascimento, F.S. Silva, Effect of laser surface texturing on primary stability and surface properties of zirconia implants, Ceram. Int. 43 (2017), https://doi.org/10.1016/j.ceramint.2017.08.058.
[23] K. Morita, N. Ishida, S. Fujimori, Y. Ishikawa, Pulsed laser processing of ceramics in water, Appl. Phys. Lett. 52 (1988) 1965–1966, https://doi.org/10.1063/1.99591.
[24] A. Kruusing, Underwater and water-assisted laser processing: Part 2—Etching, cutting and rarely used methods, Opt. Lasers Eng. 41 (2004) 329–352, https://doi.org/10.1016/S0143-8166(02)00143-4.
[25] A.N. Samant, N.B. Dahotre, Laser machining of structural ceramics—A review, J. European Ceramic Soc. 29 (6) (2009) 969–993, https://doi.org/10.1016/j.jeurceramsoc.2008.11.010.
[26] J.G. Andrews, D.R. Atthey, Hydrodynamic limit to penetration of a material by a high-power beam, J. Phys. D. Appl. Phys. 9 (1976) 2181–2194, https://doi.org/10.1088/0022-3727/9/15/009.
[27] J. Mazumder, W.M. Steen, Heat transfer model for cw laser material processing, J. Appl. Phys. 51 (1980) 941–947, https://doi.org/10.1063/1.327672.
[28] P. Fischer, V. Romano, A. Blatter, H.P. Weber, Highly precise pulsed selective laser sintering of metallic powders Nd : YAG, 55 (2005) 48–55. doi:10.1002/lapl.200410118.
[29] C.H. Fu, Y.B. Guo, Three-Dimensional Temperature Gradient Mechanism in Selective Laser Melting of Ti-6Al-4V, J. Manuf. Sci. Eng. 136 (2014) 061004, , https://doi.org/10.1115/1.4028539.
[30] P. Fischer, V. Romano, H.P. Weber, S. Kolossov, Pulsed laser sintering of metallic powders, Thin Solid Films. 453–454 (2004) 139–144, https://doi.org/10.1016/j.tsf.2003.11.152.
[31] J.M. Dixon, L.D. LaGrange, U. Merten, C.F. Miller, J.T. Porter, Electrical Resistivity of Stabilized Zirconia at Elevated Temperatures, J. Electrochem. Soc. 110 (4) (1963) 276, https://doi.org/10.1149/1.2425731.
[32] F. Wang, P. Mao, H. He, Dispensing of high concentration Ag nano-particles ink for ultra-low resistivity paper-based writing electronics, Sci. Rep. 6 (2016), https://doi.org/10.1038/srep21398.
[33] F. Wang, N. Nie, H. He, Z. Tang, Z. Chen, W. Zhu, Ultrasonic-Assisted Sintering of Silver Nanoparticles for Flexible, Electronics (2017), https://doi.org/10.1021/acs.jpcc.7b09581.
[34] S. Ogura, H. Maruyama, M. Matsubayashi, R. Ogawa, T. Nakamura, S. Komatsu, T. Isoda, Carboxylate-passivated silver nanoparticles and their application to sintered interconnection: a replacement for high temperature lead-rich solders, J. Electron. Mater. 39 (2010) 1233–1240, https://doi.org/10.1007/s11664-010-1236-y.
[35] A. Magdassi, S. Grouchko, M. Berezin, O. Kamyshny, Triggering the sintering of silver nanoparticles at room temperature, ACS Nano. 4 (2010) 1943–1948, https://doi.org/10.1021/nn901868t.
[36] S. Grouchko, M. Kamyshny, A. Mihailescu, C.F. Anghel, D.F. Magdassi, Conductive inks with a built-in mechanism that enables sintering at room temperature, ACS Nano. 5 (2011) 3354–3359, https://doi.org/10.1021/nn2005848.
[37] G. Islam, M.U. Campbell, Laser machining of ceramics: A review, Mater. Manuf. Process. 8 (1993) 611–630.
[38] M. Noda, Y. Okuda, J. Tsuruki, Y. Minesaki, Y. Takenouchi, S. Ban, Surface damages of zirconia by Nd:YAG dental laser irradiation, Dent. Mater. J. 29 (2010) 536–541, https://doi.org/10.4012/dmj.2009-127.
[39] O. Carvalho, F. Sousa, S. Madeira, F.S. Silva, G. Miranda, HAp-functionalized zirconia surfaces via hybrid laser process for dental applications, Opt. Laser Technol. 106 (2018) 157–167, https://doi.org/10.1016/j.optlastec.2018.03.017.
[40] I. Standard, Implants for surgery —Ceramic materials based on yttria-stabilized tetragonal zirconia, (Y-TZP) (2008).
[41] J.B. Quinn, G.D. Quinn, J.R. Kelly, S.S. Scherrer, Fractographic analyses of three ceramic whole crown restoration failures, Denatl Mater. J. 21 (2005) 920–929, https://doi.org/10.1016/j.dental.2005.01.006.